quently, the temperature reaches its maximum value, and then the temperature distribution converges to its final configuration v_F.

REFERENCES

[1] J. G. Short and P. F. Turner, "Physical hyperthermia and cancer therapy," *Proc. IEEE*, vol. 68, pp. 133–142, Jan. 1980.

[2] A. W. Guy, J. F. Lehamann, and J. B. Stonebridge, "Therapeutic applications of electromagnetic power," *Proc. IEEE*, vol. 62, pp. 55–75, Jan. 1974.

[3] H. S. Carslaw and J. C. Jaeger, *Conduction of Heat in Solids*. Oxford: University Press, 1959.

[4] K. R. Foster, H. N. Kriticos, and H. P. Schwan, "Effect of surface cooling and blood flow on the microwave heating of tissues," *IEEE Trans. Biomed. Eng.*, vol. BME-25, pp. 313–316, Mar. 1978.

[5] R. Paglione, F. Sterzer, J. Mendecki, E. Friedhenthal, and C. Botstein, "27 MHz ridged waveguide applicators for localized hyperthermia treatment of deep-seated malignant tumors," *Microwave J.*, pp. 71–80, Feb. 1981.

[6] M. Gex-Fabry, J. Landry, M. Marceau, and S. Gagné, "Prediction of temperature profiles in tumors and surrounding normal tissues during magnetic induction heating," *IEEE Trans. Biomed. Eng.*, vol. BME-30, pp. 271–277, May 1983.

[7] F. Bardati, "Time-dependent microwave heating and surface cooling of simulating living tissues," *IEEE Trans. Microwave Theory Tech.*, vol. MTT-29, pp. 825–828, Aug. 1981.

[8] K. R. Foster, P. S. Ayyaswamy, T. Sundaraayan, and K. Ramakrishma, "Heat transfer in surface cooled objects subject to microwave heating," *IEEE Trans. Microwave Theory Tech.*, vol. MTT-30, pp. 1158–1166, Aug. 1982.

[9] R. J. Spiegel, D. M. Deffenbaugh, and J. E. Mann, "A thermal model of the human body exposed to an electromagnetic field," *Biolectromagn.*, vol. 1, pp. 253–270, 1980.

[10] J. L. Guerkin-Kern, L. Palas, M. Samsel, and M. Gautherie, "Hyperthermie micro-ondes: Influence du flux sanguin et des phénomènes thermorégulateurs," *Bull. Cancer* (Paris), vol. 68, pp. 273–280, Mar. 1981.

[11] S. Caorsi and A. Gialdini, "Riscaldamento elettromagnetico di modelli a strati piani di tessuti biologici: In-fluenza dei fenomeni termoregolatori," in *Proc. IV Nat. Conf. Elettromagnetismo Applicato*, Florence (Italy), Oct. 4–6, 1982, pp. 105–107.

[12] S. Caorsi, "Microwave heating of biological plane layers and nonlinear thermoregulatory effects," presented at the V Annual Meeting of The Bioelectromagnetics Society, Boulder, Co., June 12–16, 1983, p. GJ–58.

[13] S. Caorsi, "Electromagnetic heating and nonlinear thermoregulatory response of biological systems," in *Proc. 1983 URSI Int. Symp. on Electromagnetic Theory*, Santiago de Compostela (Spain), August 23–26, 1983, pp. 673–676.

[14] E. H. Grant, R. J. Sheppard, and G. P. South, *Dielectric Behaviour of Molecules in Solution*. Oxford: Clarendon Press, 1978.

[15] J. B. Hasted, *Aqueous Dielectrics*. London: Chapman and Hall, 1973.

[16] A. Wexler, "Computation of electromagnetic fields," *IEEE Trans. Microwave Theory Tech.*, vol. MTT-47, pp. 416–439, Aug. 1969.

[17] D. U. Von Rosemberg, *Methods for the Numerical Solution of Partial Differential Equations*. New York: American Elsevier, 1969.

Numerical Study of the Current Distribution on a Post in a Rectangular Waveguide

YEHUDA LEVIATAN, MEMBER, IEEE, DER-HUA SHAU, AND ARLON T. ADAMS, SENIOR MEMBER, IEEE

***Abstract*—A recently developed, rapidly converging moment solution for electromagnetic scattering by a single inductive post in a rectangular waveguide is extended to include the current induced on the post surface. The results are represented by a Fourier series and the first few terms are compared with available data. The excellent agreement demonstrates that this approach can yield an accurate solution. This rather simple procedure is even more attractive when other waveguide obstacles such as thick irises and posts of arbitrary shape, which require, in general, more than just a few Fourier terms for their current representation, are encountered.**

Manuscript received December 8, 1983; revised May 21, 1984. This work was partially supported by the Technion VPR fund "Philipson Fund for Research in Electrical Engineering."

Y. Leviatan is with the Department of Electrical Engineering, Technion-Israel Institute of Technology, Haifa, Israel.

D. Shau and A. T. Adams are with the Department of Electrical and Computer Engineering, Syracuse University, Syracuse, NY 13210.

I. INTRODUCTION

In a recent paper [1], Leviatan *et al.* have formulated the problem of a single inductive post in a rectangular waveguide in terms of an equivalent current, represented by a set of unknown current filaments placed either on or inside the post surface. Further, they applied a multiple point matching of the boundary condition on the post surface and solved for the unknown filamentary currents via the method of moments. These currents have then been employed to derive the scattering matrix and the equivalent T-network parameters for the post junction. The computed results showed good agreement with Marcuvitz's data [2] as far as this data goes, and demonstrated the feasibility of using this rather simple moment approach in solving the single-post as well as a variety of microwave discontinuities.

Although this paper [1] addresses many aspects of the single-post problem, its scope has been confined to the calculation of the equivalent T-network for the post two-port junction. Little attention has been paid to the current induced on the post surface. Knowledge of the surface induced current is not solely of academic interest, but of practical importance as well. For example, this current can be used in a perturbational solution to approximate the power dissipated in an imperfectly conducting post surface.

The main objective of this paper is to show that the simple multifilamentary representation for the equivalent current can accurately predict the actually induced current. The circular post is an attractive case study because pertaining results can be readily checked against results available, although not explicitly, in [3], where the first few terms of the Fourier series representation for the current have been employed in a Galerkin procedure. A successful use of the multifilamentary representation in calculating the post current would then enable simple current calculations for other waveguide obstacles such as thick irises and posts of arbitrary shape that require, in general, more than just a few Fourier terms for their current representation.

II. FORMULATION OF THE PROBLEM

The physical configuration of the problem under study is shown in Fig. 1, together with the coordinate system used. Following the procedure suggested in [1], we replace the post by N y-directed current filaments I_i, $i=1,2,\cdots,N$ equally spaced on a circular surface S_s taken to be either the same as the post surface S_o or concentric and inside S_o as shown in Fig. 2. These filaments function as an approximate equivalent current and, as such, generate a field which is approximately the field scattered by the post itself on and external to S_o.

The surface current induced on the circular post can be readily derived from the incident and scattered magnetic fields $\boldsymbol{H}^{\text{inc}}$ and $\boldsymbol{H}^{\text{scat}}$, as follows

$$\boldsymbol{J}_s = \hat{\boldsymbol{n}} \times (\boldsymbol{H}^{\text{inc}} + \boldsymbol{H}^{\text{scat}}) \tag{1}$$

where $\hat{\boldsymbol{n}}$ is a unit vector normal to the post surface. As shown in Fig. 1, $\hat{\boldsymbol{n}}$ is pointing towards the waveguide region. Using the coordinate system depicted in Fig. 1, $\hat{\boldsymbol{n}}$ is expressed as

$$\hat{\boldsymbol{n}} = -\boldsymbol{u}_x \cos\phi + \boldsymbol{u}_z \sin\phi. \tag{2}$$

0018-9480/84/1000-1411$01.00 ©1984 IEEE

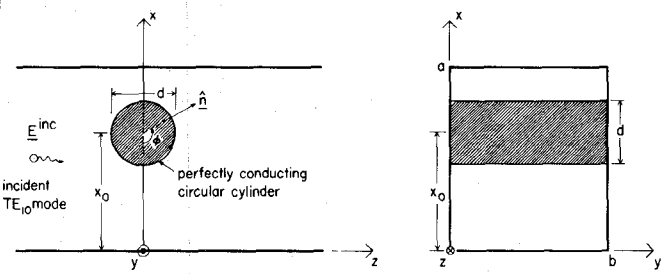

Fig. 1. Perfectly conducting circular inductive post in rectangular waveguide.

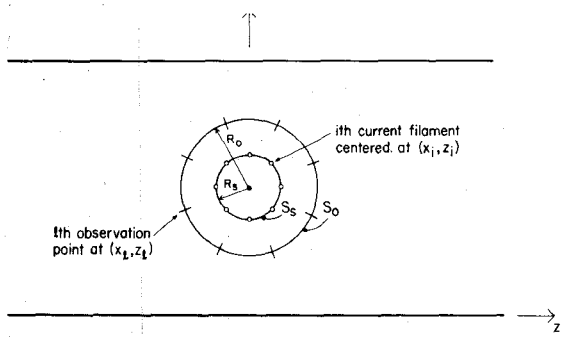

Fig. 2. Equivalent current filaments used to replace the conducting post surface.

Also, in (1)

$$\boldsymbol{H}^{\text{inc}} = \boldsymbol{u}_x H_x^{\text{inc}} + \boldsymbol{u}_z H_z^{\text{inc}} \tag{3}$$

$$\boldsymbol{H}^{\text{scat}} = \sum_{i=1}^{N} \left(\boldsymbol{u}_x H_{ix}^{\text{scat}} + \boldsymbol{u}_z H_{iz}^{\text{scat}}\right). \tag{4}$$

Here

$$H_x^{\text{inc}} = -\frac{k_{z1}}{\omega\mu} \sin\frac{\pi x}{a} e^{-jk_{z1}z} \tag{5}$$

$$H_z^{\text{inc}} = -\frac{\pi}{j\omega\mu a} \cos\frac{\pi x}{a} e^{-jk_{z1}z} \tag{6}$$

are the x and z components of the magnetic field of the incident TE_{10} mode [1, eq. (13)] and

$$H_{ix}^{\text{scat}} = \pm\frac{I_i}{a} \sum_{m=1}^{\infty} \sin\frac{m\pi x_i}{a} \sin\frac{m\pi x}{a} e^{-jk_{zm}|z-z_i|} \tag{7}$$

$$H_{iz}^{\text{scat}} = \frac{I_i}{a} \sum_{m=1}^{\infty} \frac{m\pi}{jk_{zm}a} \sin\frac{m\pi x_i}{a} \cos\frac{m\pi x}{a} e^{-jk_{zm}|z-z_i|} \tag{8}$$

are the x and z components of the magnetic field due to current filament I_i situated at (x_i, z_i). The k_{zm} are the modal wavenumbers [1, eqs. (4), (5)]. In (7), the upper sign is for $z > z_i$, while the lower sign is for $z < z_i$.

To convert the series in (7) and (8) to more rapidly converging ones, we use the two auxiliary series

$$S_{ix}^{\text{aux}} = \pm\frac{I_i}{a} \sum_{m=1}^{\infty} \sin\frac{m\pi x_i}{a} \sin\frac{m\pi x}{a} e^{-(m\pi/a)|z-z_i|} \tag{9}$$

$$S_{iz}^{\text{aux}} = \frac{I_i}{a} \sum_{m=1}^{\infty} \sin\frac{m\pi x_i}{a} \cos\frac{m\pi x}{a} e^{-(m\pi/a)|z-z_i|} \tag{10}$$

which, when summed in closed form, reduce to

$$S_{ix}^{\text{aux}} = \pm\frac{I_i}{2a} \operatorname{Re}\left\{\frac{C-D}{(1-C)(1-D)}\right\} \tag{11}$$

$$S_{iz}^{\text{aux}} = \frac{I_i}{2a} \operatorname{Im}\left\{\frac{D-C}{(1-C)(1-D)}\right\} \tag{12}$$

with

$$C = \exp\left(j\frac{\pi}{a}\left[(x-x_i)+j|z-z_i|\right]\right) \tag{13}$$

$$D = \exp\left(j\frac{\pi}{a}\left[(x+x_i)+j|z-z_i|\right]\right). \tag{14}$$

Subtracting (9) and (10) from (7) and (8) and adding the resultant expressions into (11) and (12), respectively, we obtain

$$H_{ix}^{\text{scat}} = S_{ix}^{\text{aux}} + S_{ix} \tag{15}$$

$$H_{iz}^{\text{scat}} = S_{iz}^{\text{aux}} + S_{iz} \tag{16}$$

where S_{ix} and S_{iz} are the rapidly convergent summations

$$S_{ix} = \pm\frac{I_i}{a} \sum_{m=1}^{\infty} \left(e^{-jk_{zm}|z-z_i|} - e^{-(m\pi/a)|z-z_i|}\right) \cdot \sin\frac{m\pi x_i}{a} \sin\frac{m\pi x}{a} \tag{17}$$

$$S_{iz} = \frac{I_i}{a} \sum_{m=1}^{\infty} \left(\frac{m\pi}{jk_{zm}a} e^{-jk_{zm}|z-z_i|} - e^{-(m\pi/a)|z-z_i|}\right) \cdot \sin\frac{m\pi x_i}{a} \cos\frac{m\pi x}{a}. \tag{18}$$

In terms of the preceding formulation, the current in (1) is now given by

$$\boldsymbol{J}_s = \boldsymbol{u}_y J_{sy} = \boldsymbol{u}_y \left[\cos\phi\left(H_z^{\text{inc}} + \sum_{i=1}^{N} H_{iz}^{\text{scat}}\right) + \sin\phi\left(H_x^{\text{inc}} + \sum_{i=1}^{N} H_{ix}^{\text{scat}}\right)\right]. \tag{19}$$

This current can also be expressed by the Fourier series

$$\boldsymbol{J}_s = \boldsymbol{u}_y J_{sy} = \boldsymbol{u}_y \left[\sum_{n=0}^{\infty} a_n \cos n\phi + \sum_{n=1}^{\infty} b_n \sin n\phi\right] \tag{20}$$

where

$$a_0 = \frac{1}{2\pi}\int_0^{2\pi} J_{sy}\, d\phi \tag{21}$$

$$a_n = \frac{1}{\pi}\int_0^{2\pi} J_{sy} \cos n\phi\, d\phi, \qquad n = 1,2,\cdots \tag{22}$$

$$b_n = \frac{1}{\pi}\int_0^{2\pi} J_{sy} \sin n\phi\, d\phi, \qquad n = 1,2,\cdots. \tag{23}$$

Equations (21)–(23) constitute the set of Fourier coefficients to be compared with another approximate solution [3], which hereafter is referred to as the exact solution.

III. Numerical Results

The computer program described and listed in [4] has been modified to include the preceding formulation. It should be emphasized that, while this program is applicable exclusively to the single-post obstacle, it can be generalized straightforwardly to encompass other y-independent obstacles. Only the centered post case ($x_0 = 0.5a$) is examined. Also, although results have been computed for a large number of coefficients, the information presented in the following tables is restricted to the most significant coefficients, namely, a_0, b_1, a_2, b_3, and a_4. Note that in our case a_1, b_2, a_3, and b_4 are identically zero. In all cases, the ratio λ/a is constant and equal to 1.2.

The real and imaginary parts as well as the absolute values of a_0, b_1, a_2, b_3, and a_4 are tabulated in Tables I–V for various d/a ratios. The tables reveal that, as the post diameter becomes larger (for a given waveguide width a), the relative contribution of the constant and $\sin\phi$ terms becomes smaller while the $\cos 2\phi$,

TABLE I
a_0 FOR VARIOUS d/a RATIOS ($\lambda/a = 1.2$)
(AMPERES/METER)

d/a	Re(a_0)	Im(a_0)	$\lvert a_0 \rvert$
0.1	0.005628	-0.002647	0.006219
0.2	0.003624	0.000113	0.003626
0.3	0.002325	0.000894	0.002491
0.4	0.001515	0.001119	0.001883
0.5	0.000970	0.001167	0.001517

TABLE II
b_1 FOR VARIOUS d/a RATIOS ($\lambda/a = 1.2$)
(AMPERES/METER)

d/a	Re(b_1)	Im(b_1)	$\lvert b_1 \rvert$
0.1	-0.003967	-0.000243	0.003974
0.2	-0.003484	-0.000762	0.003566
0.3	-0.002877	0.001295	0.003155
0.4	-0.002227	0.001685	0.002793
0.5	-0.001573	-0.001898	0.002465

TABLE III
a_2 FOR VARIOUS d/a RATIOS ($\lambda/a = 1.2$)
(AMPERES/METER)

d/a	Re(a_2)	Im(a_2)	$\lvert a_2 \rvert$
0.1	0.000196	0.000092	0.000292
0.2	-0.000636	-0.000020	0.000636
0.3	-0.000926	-0.000356	0.000992
0.4	-0.000982	-0.000725	0.001221
0.5	-0.000856	-0.001030	0.001339

TABLE IV
b_3 FOR VARIOUS d/a RATIOS ($\lambda/a = 1.2$)
(AMPERES/METER)

d/a	Re(b_3)	Im(b_3)	$\lvert b_3 \rvert$
0.1	0.000017	0.000001	0.000017
0.2	0.000073	0.000016	0.000075
0.3	0.000165	0.000074	0.000181
0.4	0.000259	0.000196	0.000325
0.5	0.000306	0.000369	0.000479

$\sin 3\phi$, and $\cos 4\phi$ terms gradually increase. This readily explains the need to account for more than the zeroth and first-order terms when larger posts are considered. The same trend has been noted in conjunction with the off-centered post case (not shown). Specifically, for a given d/a ratio, modal terms higher than the zeroth and first became a cardinal part of the induced current as the post approached one of the side walls.

Next, we investigate the convergence process as the number of filaments N is increased from six to 12. Many cases were treated and all show similar behavior, but only the case $d/a = 0.5$ (largest post considered), $R_s/R_0 = 0.5$ will be discussed. Here, six to 12 sources correspond to approximately five to 10 sources per one wavelength circumference. To limit the data presented,

TABLE V
a_4 FOR VARIOUS d/a RATIOS ($\lambda/a = 1.2$)
(AMPERES/METER)

d/a	Re(a_4)	Im(a_4)	$\lvert a_4 \rvert$
0.1	0.000000	0.000000	0.000000
0.2	0.000000	0.000000	0.000000
0.3	0.000007	0.000003	0.000008
0.4	0.000031	0.000023	0.000039
0.5	0.000062	0.000075	0.000097

TABLE VI
a_0 FOR VARIOUS NUMBERS OF FILAMENTS N
($\lambda/a = 1.2$, $d/a = 0.5$, $R_s/R_0 = 0.5$)
(AMPERES/METER)

N	Re(a_0)	Im(a_0)
6	0.0009506	0.0011710
7	0.0009639	0.0011688
8	0.0009672	0.0011677
9	0.0009687	0.0011673
10	0.0009692	0.0011668
11	0.0009695	0.0011667
12	0.0009696	0.0011667
EXACT	0.0009697	0.0011666

TABLE VII
b_1 FOR VARIOUS NUMBERS OF FILAMENTS N
($\lambda/a = 1.2$, $d/a = 0.5$, $R_s/R_0 = 0.5$)
(AMPERES/METER)

N	Re(b_1)	Im(b_1)
6	-0.0015795	-0.0018998
7	-0.0015623	-0.0019085
8	-0.0015694	-0.0019020
9	-0.0015711	-0.0018996
10	-0.0015720	-0.0018987
11	-0.0015722	-0.0018993
12	-0.0015724	-0.0018982
EXACT	-0.0015725	-0.0018980

TABLE VIII
a_2 FOR VARIOUS NUMBERS OF FILAMENTS N
($\lambda/a = 1.2$, $d/a = 0.5$, $R_s/R_0 = 0.5$)
(AMPERES/METER)

N	Re(a_2)	Im(a_2)
6	-0.0008915	-0.0010983
7	-0.0008658	-0.0010499
8	-0.0008601	-0.0010384
9	-0.0008574	-0.0010331
10	-0.0008564	-0.0010310
11	-0.0008561	-0.0010301
12	-0.0008559	-0.0010298
EXACT	-0.0008557	-.0010295

TABLE IX
a_0 FOR VARIOUS R_s/R_0 RATIOS
($\lambda/a = 1.2$, $d/a = 0.3$, $N = 8$)
(AMPERES/METER)

R_s/R_0	$\mathrm{Re}(a_0)$	$\mathrm{Im}(a_0)$
0.1	0.0023314	0.0008960
0.2	0.0023244	0.0008941
0.3	0.0023252	0.0008946
0.4	0.0023253	0.0008947
0.5	0.0023250	0.0008957
0.6	0.0023240	0.0008988
0.7	0.0023214	0.0009078
0.8	0.0023197	0.0009325
0.9	0.0023883	0.0010175
1.0	0.0011577	0.0005446
EXACT	0.0023254	0.0008945

TABLE X
b_1 FOR VARIOUS R_s/R_0 RATIOS
($\lambda/a = 1.2$, $d/a = 0.3$, $N = 8$)
(AMPERES/METER)

R_s/R_0	$\mathrm{Re}(b_1)$	$\mathrm{Im}(b_1)$
0.1	-0.0028872	-0.0012930
0.2	-0.0028876	-0.0012926
0.3	-0.0028876	-0.0012929
0.4	-0.0028879	-0.0012933
0.5	-0.0028886	-0.0012955
0.6	-0.0028909	-0.0013018
0.7	-0.0028970	-0.0013181
0.8	-0.0029211	-0.0013597
0.9	-0.0031159	-0.0015167
1.0	-0.0013707	-0.0007186
EXACT	-0.0028766	-0.0012950

TABLE XI
a_2 FOR VARIOUS R_s/R_0 RATIOS
($\lambda/a = 1.2$, $d/a = 0.3$, $N = 8$)
(AMPERES/METER)

R_s/R_0	$\mathrm{Re}(a_2)$	$\mathrm{Im}(a_2)$
0.1	-0.0009272	-0.0003564
0.2	-0.0009257	-0.0003561
0.3	-0.0009263	-0.0003558
0.4	-0.0009286	-0.0003573
0.5	-0.0009327	-0.0003593
0.6	-0.0009407	-0.0003638
0.7	-0.0009556	-0.0003737
0.8	-0.0009896	-0.0003979
0.9	-0.0011748	-0.0005009
1.0	-0.0004441	-0.0002089
EXACT	-0.0009258	-0.0003560

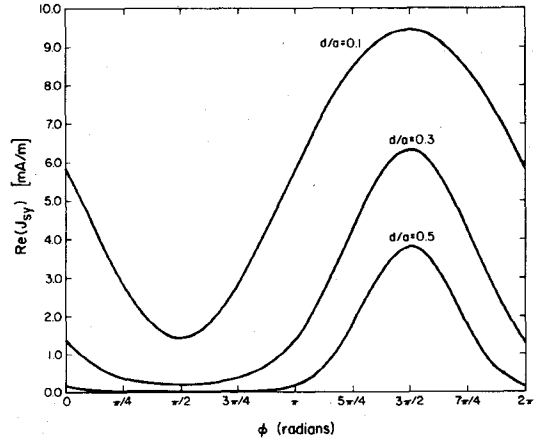

(a)

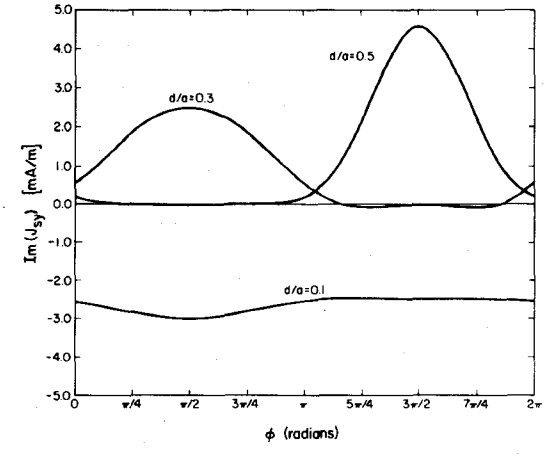

(b)

Fig. 3. (a) Plots of $\mathrm{Re}(J_{sy})$ versus ϕ for centered post in a rectangular waveguide with $\lambda/a = 1.2$ for various d/a ratios. (b) Plots of $\mathrm{Im}(J_{sy})$ versus ϕ for centered post in a rectangular waveguide with $\lambda/a = 1.2$ for various d/a ratios.

we confine our attention to a_0, b_1, and a_2, and compare pertaining results with the exact solution in Tables VI–VIII. Note that our approximate solution is less than 0.03 percent in error when 10 sources per one wavelength circumference are used.

Further, Tables IX–XI show how the values of a_0, b_1, and a_2 depend upon the choice of the circular source surface S_s. Unlike the equivalent circuit parameter, which were actually independent of the choice of S_s[1], it appears that the induced current is definitely sensitive to the ratio R_s/R_0. The data presented indicate very close agreement with the exact solution throughout the range $0.1 \leqslant R_s/R_0 \leqslant 0.6$. As expected, the agreement deteriorates when the equivalent sources approach the post surface ($R_s/R_0 = 1$).

Finally, Fig. 3 shows induced current distributions versus ϕ for various d/a ratios. Here, the interval from 0 to π on ϕ is in the "shadow" region of the post surface S_o while the π to 2π interval is in the "illuminated" portion of S_o. The current appears to be symmetric about $\phi = \pi/2$ in the former interval and symmetric about $3\pi/2$ in the latter. This is to be expected in view of the excitation and the symmetry of the centered-post structure. Note however that, in the more general case of an off-centered post, the current would not have similar symmetries.

IV. Discussion

The rapidly converging moment solution recently used to determine the equivalent circuit parameters for an inductive post obstacle in a rectangular guide [1] has been extended to treat the post surface induced currents. It was found that the multifilamentary representation of the equivalent current can provide an accurate knowledge of the actual induced current. The procedure would presumably prove useful in resolving the induced current for other waveguide obstacles such as thick irises and posts of arbitrary shape that require, in general, more than just a few Fourier terms for their current representation.

A point should be made concerning the choice of the number of filaments N. The results presented in Section III exhibit a remarkable agreement with the exact solution with a number of sources as small as 10 per one-wavelength circumference. Note that, for any engineering needs, even a smaller number of sources could suffice.

The question of appropriately choosing the circular surface S_s has been dealt with, though indirectly, in the preceding section. The studies have shown that, with a fixed number of equivalent sources, the agreement with the exact solution is excellent within the range $0.1 \leqslant R_s/R_0 \leqslant 0.6$, where the value of the parameter R_s/R_0 is virtually of no importance. However, the results do deteriorate when the equivalent sources surface S_s approaches the post surface. This behavior has been already observed in connection with a numerical solution of two-dimensional electromagnetic wave diffraction [5]. Note that this is in contrast to the equivalent network parameters that are virtually independent of the choice of S_s [1]. This cardinal difference is attributable to the stationary character of the formula for the elements of this two-port network, which renders their calculation insensitive to small variations of the current about the true current.

References

[1] Y. Leviatan, P. G. Li, A. T. Adams, and J. Perini, "Single-post inductive obstacle in rectangular waveguide," *IEEE Trans. Microwave Theory Tech.*, vol. MTT-31, pp. 806–812, Oct. 1983.

[2] *Waveguide Handbook*, N. Marcurvitz, Ed., M.I.T. Rad. Lab. Ser., vol. 10. New York: McGraw-Hill, 1951, pp. 257–262.

[3] P. G. Li, A. T. Adams, Y. Leviatan, and J. Perini, "Multiple-post inductive obstacles in rectangular waveguides," *IEEE Trans. Microwave Theory Tech.*, vol. MTT-32, pp. 365–373, Apr. 1984.

[4] Y. Leviatan, P. G. Li, A. T. Adams, and J. Perini, "Single-post inductive obstacle in rectangular waveguide," Dept. Elec. Comput. Eng., Syracuse University, Tech. Rep. TR-82-13, Nov. 1982.

[5] R. S. Popovidi and Z. S. Tsverikmazashvili, "Numerical study of a diffraction problem by a modified method of non-orthogonal series," *U.S.S.R. Comput. Math. Phys.*, vol. 17, no. 2, pp. 93–103, 1977.

Modes in Anisotropic Rectangular Waveguides: An Accurate and Simple Perturbation Approach

ARUN KUMAR, M. R. SHENOY, AND K. THYAGARAJAN

Abstract—**We present a simple and accurate perturbation method for obtaining the propagation characteristics of anisotropic rectangular waveguides described by a diagonal dielectric constant tensor. Comparison with the results of finite-element technique shows an excellent agreement.**

Manuscript received January 4, 1984; revised April 24, 1984. This work was supported in part by the Department of Science and Technology, India. One of the authors (MRS) wishes to thank the Indian Institute of Technology, Delhi, for financial support.

The authors are with the Physics Department of the Indian Institute of Technology, New Delhi—110 016, India.

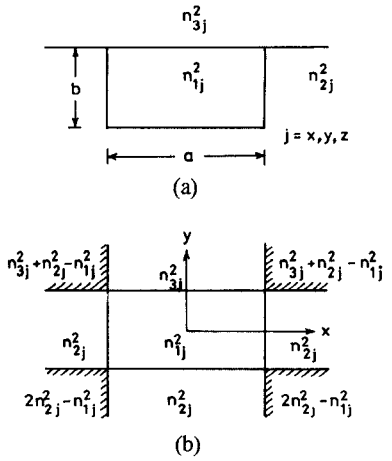

Fig. 1. (a) An embedded anisotropic channel waveguide with diagonal dielectric permittivity tensor. (b) The unperturbed structure used as a basis for obtaining the propagation characteristics of the waveguide shown in (a).

I. Introduction

The basic structural element common to many of the integrated optic devices is a single-mode channel waveguide. For an efficient design of devices, such as directional couplers, filters, and modulators, that are generally fabricated on an anisotropic substrate like $LiNbO_3$ [1], it is important to study the modal properties of anisotropic channel waveguides—the simplest of these consists of a homogeneous rectangular core. Achieving exact analytical solutions of such waveguides presents considerable difficulty, even for the isotropic case, due to the presence of corners. Numerical methods like the finite-element technique have been used for studying such problems [2]–[4]; however, these involve extensive and time-consuming computer calculations. Some approximate analytical techniques have also been presented [5], [6]; the effective index method [6] which can also be used for homogeneous core waveguides, has been shown to sometimes give ambiguous results [7]. The technique presented in [5] involves solving coupled transcendental equations, and also neglects the effect of corners, which, as we will show, becomes important near cutoff and for near-square cross section core waveguides.

In this paper, we present a simple and accurate method to obtain the propagation constants and the modal fields in homogeneous anisotropic channel waveguides described by a diagonal dielectric constant tensor. The results are compared with the finite-element method, and it is shown that our method gives highly accurate results, particularly for the fundamental modes.

II. Method

We consider a homogeneous anisotropic channel waveguide with each region characterized by a diagonal dielectric constant tensor. The principal dielectric constants of the core are denoted by $n_{1x}^2, n_{1y}^2, n_{1z}^2$, and the substrate by $n_{2x}^2, n_{2y}^2, n_{2z}^2$ (see Fig. 1). In each region, the electric field satisfies the following equation:

$$\nabla(\nabla\cdot\boldsymbol{E}) - \nabla^2\boldsymbol{E} = k_o\hat{k}\boldsymbol{E} \qquad (1)$$

where k_o is the free-space wavenumber and $\hat{k}$ represents the dielectric constant tensor.

The modes in channel waveguides can be classified into E_{pq}^y (polarized predominantly along the y-direction) and E_{pq}^x (polarized predominantly along the x-direction) modes [4], [6],

0018-9480/84/1000-1415$01.00 ©1984 IEEE